

3D non-hydrostatic modelling of bottom stability under impact of the turbulent ship propeller jet

Igor BROVCHENKO¹, Julia KANARSKA², Vladimir MADERICH¹
and Katerina TERLETSKA¹

¹ Ukrainian Center of Environmental and Water Projects
Glushkova Prospect 42, 03187, Kiev, Ukraine
e-mail: brovchik@env.kiev.ua

² Institute of Geophysics and Planetary Physics UCLA
405 Hilgard Ave., Los Angeles, CA 90095, USA

A b s t r a c t

New three-dimensional numerical non-hydrostatic model with a free surface that was designed for modelling the bottom and bank stability subjected by ship propeller jets is presented. Unlike all known models, it describes three-dimensional fields of velocities generated by ship propellers, turbulence intensity and length scale in the given domain of arbitrary bottom and coastal topography. Results of simulations are compared with the laboratory experiments.

Key words: non-hydrostatic model, turbulent propeller jet, bottom erosion.

1. INTRODUCTION

Propeller jets from the moving vessels in narrowings and in shallow waters can cause bottom erosion, affect the bank stability and damage the bottom habitat such as macrophytes, mussels and other macro invertebrates. That is the motivation for developing and testing a 3D non-hydrostatic free-surface hydrodynamic model NHJET that was designed for modelling of bottom and bank stability subjected by ship propeller jets. Unlike all known models, it describes three-dimensional fields of velocities generated by ship propellers, turbulence intensity and length scale in the given domain of arbitrary bottom and coastal topography. The model can describe near field in propeller jet as well as far field. The time and space varying bottom shear stresses that cause bottom erosion and damage for bottom habitat can be calculated. Simplified version of

the model allows calculation of hydrodynamic fields caused by propeller jet of a non-moving vessel. The model was developed on the basis of non-hydrostatic model of Kanarska and Maderich (2003), that is a non-hydrostatic extension of the well-known Princeton Ocean Model (POM) described by Blumberg and Mellor (1987). The main features of the model are: use of the generalized vertical coordinate system (Ezer and Mellor 2004), curvilinear orthogonal horizontal coordinate system, decomposition and calculation of the velocity and pressure on hydrostatic and dynamic components. Results of calculations were compared with laboratory experiments data (Schokking 2002).

2. APPROACH AND METHODS

Model equations

In the model, the 3D Reynolds averaged Navier–Stokes (RANS) equations are used:

$$\begin{aligned} \frac{\partial u_i}{\partial x_i} &= 0, \\ \frac{\partial u_i}{\partial t} + u_j \frac{\partial u_i}{\partial x_j} &= -\frac{1}{\rho_0} \frac{\partial p}{\partial x_i} - \frac{\partial \overline{u_i u_j}}{\partial x_j} - g_i, \end{aligned} \quad (1)$$

where $x_i = (x, y, z)$ are the Cartesian coordinates, axis z is directed upward, $u_i = (u, v, w)$ are components of averaged velocity; p is the pressure; $g_i = (0, 0, g)$ is the gravity; ρ_0 is the constant density in Boussinesq approximation. The Reynolds stresses $\overline{u_i u_j}$ are modelled using the eddy viscosity approach:

$$\overline{u_i u_j} = -K_M \left(\frac{\partial u_i}{\partial x_j} + \frac{\partial u_j}{\partial x_i} \right) + \frac{q^2 \delta_{ij}}{3}, \quad (2)$$

δ_{ij} is a Kronecker symbol, where eddy viscosity coefficient K_M is related with kinetic energy of turbulence $q^2/2$ and length scale l :

$$K_M = S_M q l, \quad (3)$$

where $q^2/2 = \overline{u_i u_i}$, and $S_M = 3A_1(1/3 - 2A_1/B_1 - C_1)$.

3D extension of q^2 - $q^2 l$ turbulence model (Mellor and Yamada 1982) is used:

$$\frac{\partial q^2}{\partial t} + u_j \frac{\partial q^2}{\partial x_j} = \frac{\partial}{\partial x_j} \left[S_q q l \frac{\partial q^2}{\partial x_j} \right] + K_M P - 2 \frac{q^3}{B_1 l}, \quad (4a)$$

$$\frac{\partial q^2 l}{\partial t} + u_j \frac{\partial q^2 l}{\partial x_j} = \frac{\partial}{\partial x_j} \left[S_l q l \frac{\partial q^2 l}{\partial x_j} \right] + 2E_1 l K_M P - \frac{q^3}{B_1} \left(1 + E_2 \left[\frac{1}{\kappa L} \right]^2 \right), \quad (4b)$$

where P is the turbulent production due to the velocity shear:

$$P = \left(\frac{\partial u}{\partial y} + \frac{\partial v}{\partial x} \right)^2 + \left(\frac{\partial u}{\partial z} + \frac{\partial w}{\partial x} \right)^2 + \left(\frac{\partial v}{\partial z} + \frac{\partial w}{\partial y} \right)^2. \quad (5)$$

Unlike one-dimensional turbulence model (Mellor and Yamada 1982), the production term includes horizontal velocity shear. In the last term in the square brackets in eq. (4), there is presented the so-called wall function that is necessary in q^2 - q^2l model for more accurate flow description near the solid boundaries. L is supposed to be a measure of the distance from the wall and specified according to

$$L^{-1} = \frac{1}{2\pi} \iint \frac{dA(\mathbf{r}_0)}{|\mathbf{r} - \mathbf{r}_0|^3} \quad (6)$$

where \mathbf{r} is the radius vector for the point in the fluid domain bounded by solid wall at \mathbf{r}_0 ; $dA(\mathbf{r}_0)$ is an elemental wall area. If the vertical scale of computational domain is negligible then the following relations can be used

$$L^{-1} = |z|^{-1} + |H + z|^{-1}, \quad (7)$$

where H is the bottom depth. In the turbulence model, eqs. (2)-(4), L calculated as minimal distance from the point to the nearest wall of the domain. The constants of turbulence model $A_1, A_2, B_1, C_1, E_1, E_2, S_q, S_l, \kappa$ are determined in Mellor and Yamada (1982).

Boundary conditions

The kinematic condition on the water surface $z = \eta(x, y, t)$ is

$$\frac{\partial \eta}{\partial t} + u \frac{\partial \eta}{\partial x} + v \frac{\partial \eta}{\partial y} = w.$$

The dynamic condition is $K_M \partial \mathbf{V}_h / \partial z = \boldsymbol{\tau}_0 / \rho_0$, where $\mathbf{V}_h = (u, v)$, $\boldsymbol{\tau}_0 = (\tau_{0x}, \tau_{0y})$ is surface stress.

At the computational layer nearest to the bottom, $z = -H + z_b$, we have:

$$-u \frac{\partial H}{\partial x} - v \frac{\partial H}{\partial y} = w, \quad K_M \frac{\partial \mathbf{V}_h}{\partial z} = \boldsymbol{\tau}_b / \rho_0,$$

where $\boldsymbol{\tau}_b = \rho_0 C_D |\mathbf{V}_h| \mathbf{V}_h$, $C_D = \max \left[0.0005; \frac{1}{\kappa} \ln \left(\frac{z_b + z_0}{z_0} \right)^{-2} \right]$, z_b is the height of the first computational point in the boundary layer, and z_0 is the roughness parameter.

The relevant boundary conditions for eqs. (2)-(4a, b) at the surface and bottom are

$$\left[q^2(\eta), q^2l(\eta) \right] = \left[B_1^{2/3} u_*^2(0), 0 \right], \quad \left[q^2(-H), q^2l(-H) \right] = \left[B_1^{2/3} u_*^2(-H), 0 \right],$$

where $u_*(0)$, $u_*(-H)$ are the dynamic velocities:

$$u_*^2(0) = |\tau_0|/\rho_0, \quad u_*^2(-H) = |\tau_b|/\rho_0.$$

At the solid boundaries, the non-slip conditions and conditions for the wall logarithmic boundary layer are used. On the jet-side boundaries, normal components of velocity and turbulence fluxes are nil, except of directly the jet domain. At the open boundaries, the condition based on Newtonian relaxation technique for a sea level is used. The computational domain is a closed area that is divided into internal zone and relaxation zones along the open boundaries. The boundary conditions at the outer boundary of relaxation zones are non-slip conditions. The equation for surface elevation was derived by the integration of continuity equation from bottom to surface. The modified equation is

$$\frac{\partial \eta}{\partial t} + \frac{\partial \bar{u}(H + \eta)}{\partial x} + \frac{\partial \bar{v}(H + \eta)}{\partial y} = -\frac{\alpha(\eta - \eta_B)}{T}. \quad (8)$$

The right-hand side is Newtonian relaxation term, where α is the relaxation parameter, that is, $\alpha = 1$ in the relaxation zone and $\alpha = 0$ outside of it, η_B is the prescribed elevation on the boundary and T is relaxation time. This parameter is chosen to satisfy non-reflecting condition for disturbances incoming in the relaxation zone.

Jet from the ship propeller

For the calculation of the inflow velocity induced by propeller jet, relations based on the empirical model (Blaauw and Van de Kaa 1987) were used. In this model the real propeller was replaced by bowthruster. The beginning of the vessel movement is considered. Thus, jet velocity U_0 is calculated as

$$U_0 = \sqrt{8K_T n^2 D^2 / \pi}, \quad (9)$$

where D is the diameter of the propeller (in m), n is the number of revolutions per second, K_T is the thrust coefficient. In case the value of K_T is unknown Blaauw and Van de Kaa give a formula for U_0 based on the installed engine power P (in wat):

$$U_0 = C_2 \left(\frac{P}{\rho_0 D_p^2} \right)^{1/3}, \quad (10)$$

where empirical constant $C_2 = 1.48$.

Numerical method

A generalized coordinate system (Ezer and Mellor 2004) is used. Pressure and velocity fields are decomposed into hydrostatic and non-hydrostatic components (Kanarska and Maderich 2003). Finite difference semi-implicit methods were used to solve 2D

equations for surface elevation and depth averaged velocities (external mode) and 3D equations for velocity and pressure (internal mode) (Blumberg and Mellor 1987). Free surface elevation, hydrostatic and non-hydrostatic components of pressure and velocity are calculated at sequential stages. Unlike most of non-hydrostatic models, 2D depth-integrated momentum and continuity equations were integrated explicitly with the mode splitting technique at the first stage, whereas the 3D equations were solved implicitly at subsequent stages.

The finite-difference solutions of governing equations were derived using a four-stage procedure. **Stage 1:** The scalar fields. Turbulent energy and length scale are computed using a semi-implicit numerical scheme. **Stage 2:** Free surface elevation. The calculation of free surface elevation is performed explicitly from depth-integrated shallow water equations. The initial 2D velocity fields on each external stage are determined by direct integration of the general non-hydrostatic 3D velocity fields of the previous internal step. **Stage 3:** Hydrostatic components of the velocity and pressure fields. The 3D hydrodynamic equations without the non-hydrostatic pressure component are solved semi-implicitly with an internal time step to determine provisional values of the velocity field. The advection and horizontal viscosity are discretized explicitly. The obtained three-diagonal system is solved by a direct method. **Stage 4:** Non-hydrostatic components of the velocity and pressure fields. The non-hydrostatic components of velocity are computed by correcting the provisional velocity field with the gradient of non-hydrostatic pressure to satisfy the continuity equation for the sum of hydrostatic and non-hydrostatic velocities. The discretized Poisson equation obtained for the non-hydrostatic pressure is reduced to a non-symmetric 15-diagonal linear system that is solved by preconditioned biconjugate gradient method. Once the non-hydrostatic pressure is determined, the corresponding components of velocity fields are calculated.

3. RESULTS

Example of simulations

Comparison of the numerical results and results of the laboratory experiment (Schokking 2002) was carried out, and the impact of the turbulent ship propeller jet on the inclined bottom was investigated. Experimental setup is presented in Fig. 1. The basin used has the dimensions $2 \times 1.9 \times 0.48$ m, the slope ratio is 1:3.

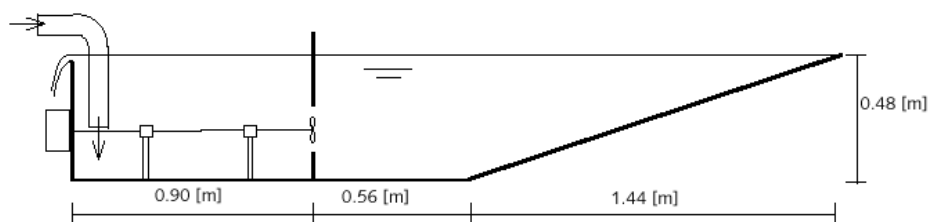


Fig. 1. Side view and dimensions of the experimental basin.

Propeller with diameter $D_0 = 0.1$ m was installed on a depth of 0.29 m in barrier that divided enclosed volume from the accessory volume in which water comes to balance level in both tanks. The water flows away through outlets on the sides of the basin, and on these sides the Newton relaxation boundary conditions was used in simulations (Palma and Matano 1996).

In the experiment, the initial velocity was $U_0 = 1.36$ m/s. In numerical simulations the jet flowed out from rectangular hole with the dimensions 10.8×6.6 cm with the initial velocity 1.38 m/s, that correspond to momentum of the flow in the experiment. The numerical grid was $100 \times 80 \times 50$ nodes. Results of the calculations of the steady flow are shown in Figs. 2 and 3. In Fig. 2 the velocity field near bottom layer when the flow become steady is shown. In Fig. 3 comparison of the calculated and experimental horizontal velocity profiles in the nearest zone (a zone of flow establishment) and distant zone (a zone of established flow) are presented. As it is seen from the figure, the calculated velocity distribution rather well agreed with experimental one. Figure 5 shows the shear stresses field near the bottom. As it seen from the pic-

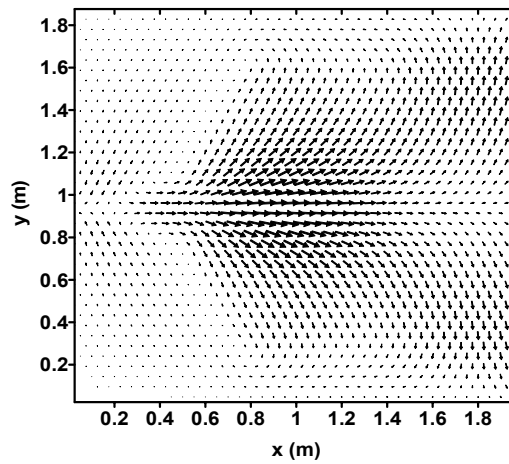


Fig. 2. Velocity field in the bottom layer.

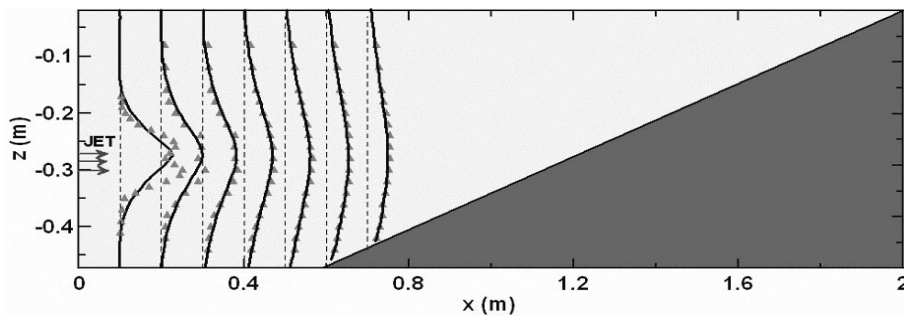


Fig. 3. Comparison of the experimental and calculated horizontal velocity profiles.

ture the zone of maximum tangential near bottom stresses is located near the point of the intersection of the jet axis and inclined bottom. The results of the free-propeller jet in the experiment of Schokking (2002) show that the maximum damage on the slope occurs at the lower part of the slope, approximately between 0 and 0.10 m from the toe (see Figs. 4 and 5a).

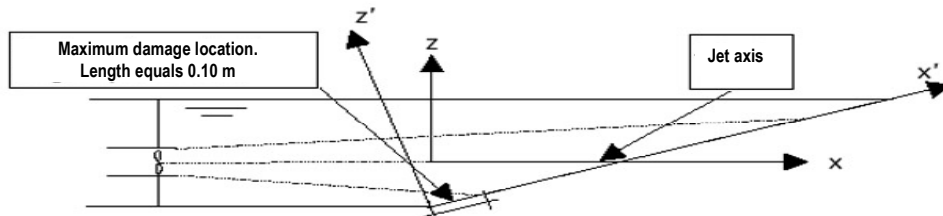


Fig. 4. Location of maximum damage, visualized in the xz plane.

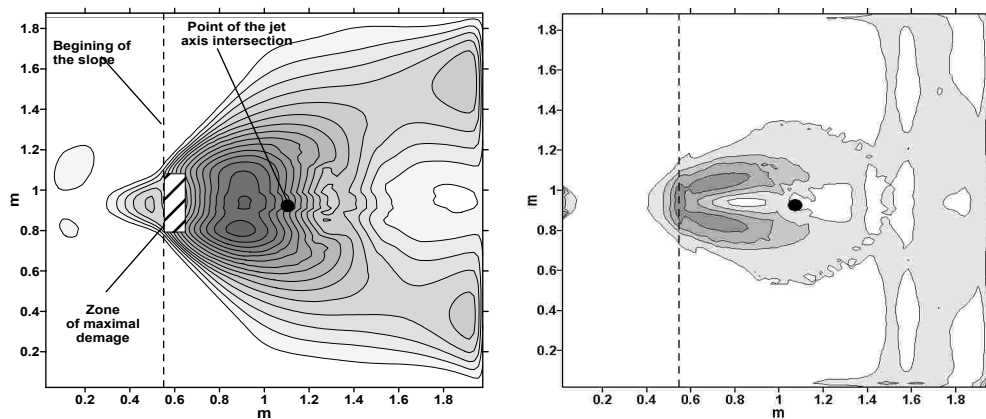


Fig. 5: (a) Bottom shear velocity field; (b) Dynamic pressure gradient module.

According to the experiments, the maximum damage zone is located much lower than the maximum bottom velocity and shear stresses zone. Moreover, the bottom sediment particle motion in the lower part of the slope occurred in the direction opposite to flow. In the framework of the model presented here the problem of the bottom erosion is not considered. However, the overview of the existing sediment transport models (Jia and Wang 1997, Donnell 2001, Mike-21 CAMS 2003) shows that most of them are based on the calculation of the equilibrium sediment concentration that is dependent only on the bottom shear stresses. Therefore, sediment transport models that takes into account only bottom shear stresses are unable to describe the location of the maximum damage zone in this experiment. Distribution of the module of the dynamic pressure gradient (see Fig. 5b) allows to explain experimental location of the maximum damage zone. The force induced by the pressure difference also is a driving force for the sediment load.

From Fig. 5b it is seen that pressure gradient has the maximum at the base of the slope and directed against the flow, that allows to explain the direction and mechanism of particles motion in the experiment.

4. CONCLUSIONS

A new three-dimensional numerical non-hydrostatic model with a free surface is presented that was designed for modelling bottom and bank stability subjected by ship propeller jets. As distinct from all known models, it describes three-dimensional fields of velocities generated by ship propellers, turbulence intensity and length scale in the given domain of arbitrary bottom and coastal topography. The time and space varying bottom shear stresses and pressure gradient are calculated. The results of simulations show agreement with laboratory experiments. It was concluded that in considered problems for bottom erosion modelling it is needed to use the models of the sediment transport that take into account forces caused by pressure gradient. Such model should be coupled with three-dimensional non-hydrostatic hydrodynamics models.

Acknowledgments. This study was partially supported by US Civil Research and Development Foundation (project UKG2-582-KV-05).

References

- Blaauw, H.G., and E.J. van de Kaa, 1978, *Erosion of bottom and sloping banks caused by the screw-race of maneuvering ships*, Proc. 7th Intern. Harbour Congress, Antwerp, May 22-26, 1978.
- Blumberg, A.F., and G.L. Mellor, 1987, *A description of a three-dimensional coastal ocean model*. In: N.S. Heaps (ed.), "Three Dimensional Coastal Ocean Models", 1-16, American Geophysical Union, Washington, DC.
- Donnell, B.P., 2001, *Users Guide to SED2D WES Version 4.5*, 164 pp., Engineer Research and Development Center Waterways Experiment Station Coastal and Hydraulics Laboratory.
- Ezer, T., and G.L. Mellor, 2004, *A generalized coordinate ocean model and a comparison of the bottom boundary layer dynamics in terrain-following and in z-levels grids*, Ocean Modelling **6**, 379–403.
- Jia, Y., and S. Wang, 1997, *CCHE2D: a two-dimensional hydrodynamic and sediment transport model for unsteady open channel flows over loose bed*, Techn. Report: No. CCHE-TR-97-2, School of Engineering, The University of Mississippi, 38 pp.
- Kanarska, Y., and V. Maderich, 2003, *A non-hydrostatic numerical model for calculating free-surface stratified flows*, Ocean Dynamics **53**, 176-185.
- Mellor, G., and T. Yamada, 1982, *Development of a turbulence closure model for geophysical fluid problems*, Reviews of Geophysics and Space Physics **20**, 851-875.

- Mike-21 CAMS, 2003, *Coastal Area Morphological Shell*, DHI Water & Environment, Users Guide, 96 pp.
- Palma, E.D., and R.P. Matano, 1996, *On the implementation of open boundary conditions to a general circulation model: The barotropic model*, J. Geophys. Res. **103**, 1319-1341.
- Schokking, L., 2002, *Bowthruster-induced Damage*, MSc Thesis, Technical University Delft, 143 pp.

Received 19 September 2006

Accepted 30 October 2006